Electronic Supplementary Material (ESI) for Physical Chemistry Chemical Physics.

Supporting Information: Polarization-Driven Catalysis via Ferroelectric Oxide Surfaces

Arvin Kakekhani[1,2,5,6*] and Sohrab Ismail-Beigi[1,2,3,4*]

[1]Department of Physics, [2]Center for Research on Interface Structure and Phenomena (CRISP),[3]Department of Applied Physics, [4]Department of Mechanical Engineering and Materials Science, Yale University, New Haven, CT 06520, [5]Department of Chemical Engineering, [6]Center for Interface Science and Catalysis (SUNCAT), Stanford University, Stanford, CA 94305, USA

E-mail: kake@stanford.edu\\sohrab.ismail-beigi@yale.edu

Pseudopotentials

We employ ultrasoft (Vanderbilt) pseudopotentials for the first principles density functional theory (DFT) calculations. Below, Table 1 provides the parameters describing the pseudopotentials: the reference valence configuration used during its generation and the cutoff radii for each angular momentum channel.

Supercell Calculation Details

In our DFT calculations, we start all the relaxation calculations by breaking symmetries in both spatial and magnetic degrees of freedom. For each system, we consider several (sometimes up to 14) initial structures, to make it as likely as possible that the lowest energy structure we find is the global minimum in energy and not just a local minimum.

Table 1: Parameters describing the pseudopotentials. Reference valence configuration and the cutoff radii for each angular momentum channel.

Atom	Reference state	r^s_{cut} (bohr)	r^p_{cut} (bohr)	r^d_{cut} (bohr)
O	$2s^2 2p^4$	1.30	1.30	—
Pb	$5d^{10} 6s^2 6p^2$	2.50	2.50	2.30
Ti	$3s^2 3p^6 3d^2 4s^2 4p^0$	1.80	1.80	2.00
H	$1s^1$	0.80	—	—
Pt	$5d^9 6s^1 6p^0$	2.26	2.32	2.00
C	$2s^2 2p^2$	1.50	1.54	—
S	$3s^2 3p^4$	1.70	1.70	—

A sample c(2×2) supercell is shown in Fig. 1 which is the unit cell used in most of our calculations. We fix the structure of the second, third and fourth atomic layers of PTO on top of the Pt electrode to their "bulk values" in order to simulate the mechanical boundary conditions appropriate to a thick ferroelectric PTO film: this leads to reasonable computational expenses and sizes of the simulation cells[1,2]. By "bulk values", we mean the appropriate DFT-minimized configuration that corresponds to crystalline PTO bi-axially strained to $SrTiO_3$ and with ferroelectric polarization pointing in the desired direction along (001).

As can be seen in Table 2, the structure of a five atom primitive $PbTiO_3$ cell depends on the plane wave cutoff E_{cut} and it is not well converged at E_{cut} = 30 Ry. One might think that in order to investigate PTO surface chemistry precisely, an E_{cut} higher than 30 Ry is needed. Obviously, one can do this and thereby increase the computational cost. However, as we are interested in precise binding energies, one should instead investigate the sensitivity of the surface binding to the cutoff and the PTO structure. Table 3 shows that, for a precision of 0.1 eV in binding energy, one must use the well-converged bulk configuration (high E_{cut} bulk structure) for the for 3 fixed layers of PTO, but it is not important whether we relax the remainder of the structure using a cutoff energy of 30 Ry or higher. Based on this observation, we choose the atomic configuration of our fixed layers to be that of the bulk at 80 Ry and then relax the remainder of the structure using E_{cut}= 30 Ry.

As can be seen in Fig. 1, we have used 4 unit cells of PTO stacked in the z-direction per 1×1 surface unit cell. Fig. 2 shows the projected density of states (PDOS) on the surface Ti atom (on the Ti-terminated surface), which is very well converged at a thickness of 3.5 unit cell of PTO.

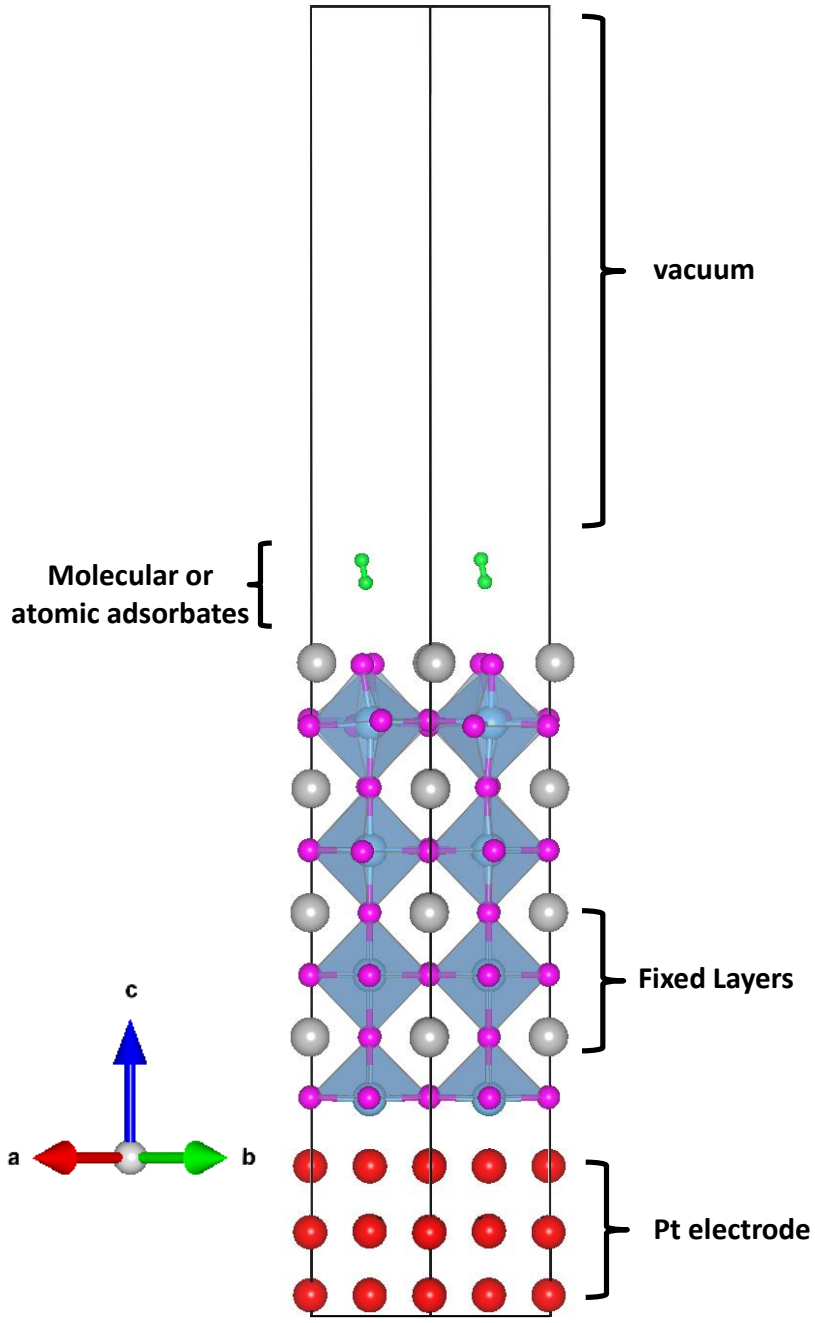

Figure 1: A sample c(2×2) unit cell used in our calculations. Gray balls are Pb, fuchsia balls are O, green balls are H, blue Ti balls are encaged in the blue octahedra formed by the O, and Pt atoms that are used as an electrode at the bottom of the cell are shown in red. Each supercell contains at least 15 Å of vacuum to isolate periodic copies of the slab in the z (i.e., c or (001)) direction.

Table 2: Sensitivity of PTO bulk structure to the plane wave cutoff E_{cut} .

PTO structure at different E_{cut}	a	c/a
30 Ry	3.89	1.12
40 Ry	3.83	1.23
50 Ry	3.84	1.22
60 Ry	3.83	1.24
80 Ry	3.84	1.23

Table 3: Sensitivity of binding energies (per adsorbate) to the structure chosen for fixed layers, and free layers on Ti-terminated PTO.

E_{cut} used for fixed and free layers	Energy cost to create 0.5 ML O vacancy (eV)
30 Ry bulk structure for fixed layers, rest relaxed at 30 Ry	2.6
40 Ry bulk structure for fixed layers, rest relaxed at 30 Ry	2.3
40 Ry bulk structure for fixed layers, rest relaxed at 40 Ry	2.3

Effect of Exchange-Correlation Functional

Here, we investigate the sensitivity of our main results (derived using the PW91 GGA functional) to the specific exchange-correlation (XC) being used. We compare PW91 to the PBE GGA[3,4] as well as to Perdew-Zunger (PZ) LDA functional[5]. As Table 4 shows, changing the XC from PW91 to PBE changes the binding energies by no more than 0.3 eV per molecule which is small compared to the absolute value of binding energies. Systematically comparing LDA to GGA results is not as straightforward. As can be seen in Table 5, GGA and LDA XC functionals predict different structures for bulk PTO. Although the in-plane lattice constants are almost identical, the out of plane lattice constant (c) and the ferroelectric atomic displacements are predicted to be larger by the GGAs. Consequently, we have two different effects to consider. First is the direct effect which is the difference in binding energies caused by changing the XC functional at fixed PTO polarization. Second is the indirect effect which is the change in binding energies originating from different PTO polarization magnitudes that the functionals predict. In order to distinguish between these two effects, we have performed four sets of calculations shown in Table 6. First, "fully GGA" calculations where we use GGA for both obtaining the structure of 3 fixed atomic layers as well in relaxing the remaining layers. Second, a set of calculations where we use the

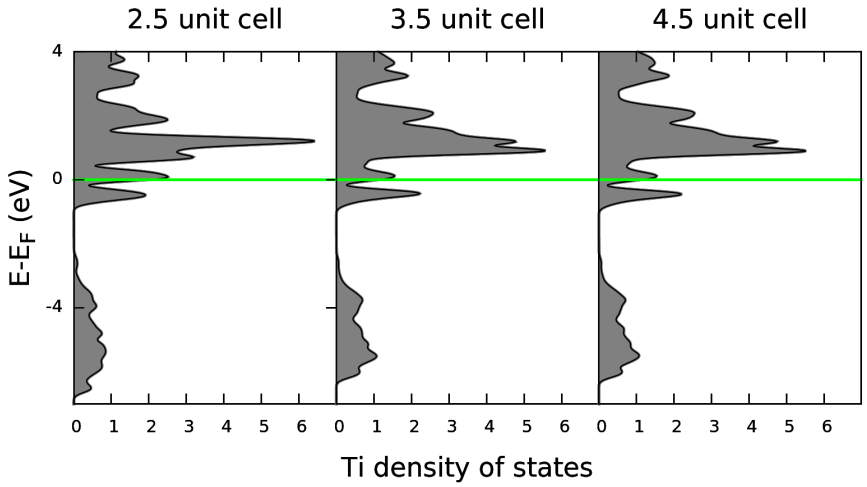

Figure 2: Projected density of states on a surface Ti atom in positively polarized Ti-terminated PTO as a function of number of unit cells of PTO. Electronic structure of the surface is well converged at a thickness of 3.5 unit cell or more.

GGA predicted structure for the fixed layers bulk and use the LDA functional to relax the system. Third, we reverse order: LDA predicted structure for the fixed layers and GGA relaxation. And fourth, LDA for all layers.

Table 4: Shows the binding energy of NO and O_2 (at 0.5 ML coverage) on two different facets of PTO and for two polarization states (positive + and negative -) using two different GGA XC functionals.

GGA flavor	NO on Pb term(eV)		NO on Ti term (eV)		O_2 on Pb term (eV)	
	+	-	+	-	+	-
PW91	1.5	1.9	3.0	2.0	2.4	0.0
PBE	1.2	1.9	2.7	2.1	2.1	-0.1

Comparing the first and the second sets of calculations in Table 6, LDA overestimates the binding energy by 0.2-0.9 eV relative to PW91 (for the same polarization of the fixed layers). This overbinding of LDA is well known and discussed in the literature[6]. Comparing the first and third sets of calculations, we note that our binding energies decrease in the latter as a result of the decreased ferroelectric displacement amplitude in the fixed layers, but this difference is no more than 30% of the absolute value of the binding energies. Comparing fully LDA calculations with fully PW91 calculations reveals that the decrease in binding energy caused by decrease in polarization in the former is to some extent compensated by the intrinsic overestimation of binding energies with LDA, so fully LDA and fully PW91 results are closer to each other, and in the worst

Table 5: The dependence of bulk ferroelectric structure (at E_{cut} 80) of PTO on the XC functional being used.

Structural parameters	LDA-PZ	GGA- PW91	GGA-PBE
a (Å)	3.86	3.84	3.84
c/a	1.04	1.23	1.23
Ti-O displacement (Å)	0.28	0.52	0.52
Pb-O displacement (Å)	0.35	0.86	0.89

case they are 0.7 eV different which is no more than 30% of the absolute value of the binding energies . Using GGA is known to give much better results for binding energies than LDA[6,7], so the range of error caused by XC functional is estimated to be the difference between the results of PBE and PW91 functionals which are no worse than 0.3 eV, which does not change the main conclusions and the processes proposed in our work.

Table 6: Four sets of calculations that investigate the change of binding energies (in eV) due to the exchange correlation functional being either GGA-PW91 or LDA-PZ.

Type of the XC functional	NO on Pb-term. (+)PTO	O_2 on Pb-term. (+)PTO	NO on Ti-term. (-)PTO
Fully GGA	1.5	2.4	2.0
GGA structure for fixed layers, rest LDA	1.7	2.8	2.8
LDA structure for fixed layers, rest GGA	1.0	2.0	1.8
Fully LDA	1.3	2.1	2.7

Geometric Reconstructions: Positively Poled $PbTiO_3$

As mentioned above, positive and negative ferroelectric polarization induce oxidizing and reducing surface chemistry, respectively. Thus, in agreement with the theoretical and experimental literature, these ferroelectric surfaces experience atomic reconstructions which change the surface stoichiometry[1,2,8–14]. For example, oxygen atoms adsorb on the positively poled (electron-doped) surface while oxygen vacancies form on the negatively poled (hole-doped) surface. Another class of reconstructions that can occur in parallel to non-stoichiometric atomic reconstructions is geometric reconstruction in which the surface stoichiometry is unchanged but the surface atoms reconfigure.

This typically includes symmetry breaking that pushes bonding states further below and anti-bonding states further above the Fermi level (E_F)[1,15], similar in spirit to a Peierls distortion[16–19]. Below we examine one such geometric reconstruction on the positively poled surface, and taking this as an example, elucidate how the out-of-plane ferroelectric polarization can induce a surface geometric reconstruction. This energy-lowering reconstruction is present in almost all the results of the main text concerning positively poled stoichiometric PTO.

Our DFT calculations indicate that the positively poled stoichiometric Pb-terminated PTO surface experiences two types of geometric reconstructions: 1) sliding of the surface Pb layer relative to the surface oxygens by half a unit cell (see Fig. 3), and 2) dimerization of the surface Pb atoms (see Fig. 6). The former lowers the surface energy by about 0.6 eV (per 1×1 surface unit cell) while the later further lowers it by about 0.1 eV (per 1×1 surface unit cell).

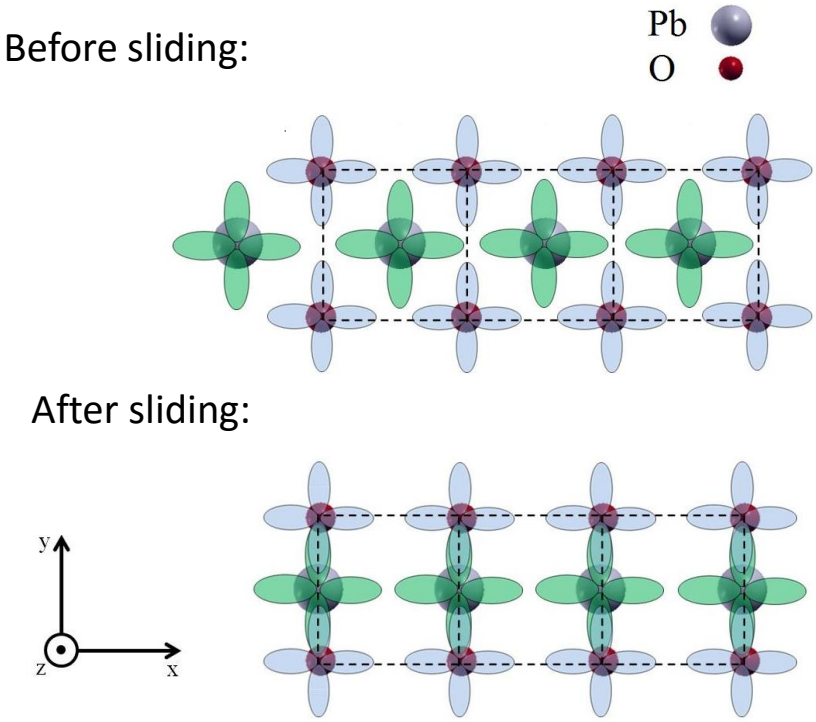

Figure 3: A top view of the sliding of the top Pb layer on (001) PTO in the x direction by half a lattice constant (along with moving up in the z direction by about 0.5 Å) . Here the green orbitals are Pb $6p_x$ and $6p_y$ orbitals and the blue orbitals are O $2p_x$ and $2p_y$ orbitals.

We begin by studying the sliding effect. The surface conduction band in Pb terminated PTO is mostly formed by Pb 6p states, while the valence band mostly consists of O 2p states (see Fig. 4). In the perovskite structure, the conduction Pb 6p bands are shifted up in energy (antibonding

states) by hybridizing with the valence O 2p sates while the valence O 2p bands are pushed down in energy (bonding states). Separately, the existence of the out-of-plane polarization in positive direction dopes electrons to the surface. Thus on positively poled surface, the Fermi level lies inside the conduction band (see Fig. 4 (a)). As Fig 3 shows, sliding the top Pb atoms in the x direction decreases the overlap of Pb $6p_x$ and O $2p_x$ orbitals while increasing the overlap of Pb $6p_y$ and O $2p_y$ orbitals. This causes Pb $6p_x$ orbitals to drop lower, O $2p_x$ to shift higher, Pb $6p_y$ to shift higher and O $2p_y$ to shift lower in energy (see Fig. 4). Before sliding, by symmetry there is no difference between Pb $6p_x$ and Pb $6p_y$: the left side of Fig. 4 shows that these two projections overlap and the center of both is 1.7 eV above E_F; the center of the overlapping O $2p_x$ and O $2p_y$ projections is 4.5 eV below E_F. After sliding, the center of Pb $6p_x$ and Pb $6p_y$ are accordingly at 1.2 and 2.4 eV above E_F which agrees with the prediction above. The center of O $2p_x$ and O $2p_y$ are accordingly at 4.4 and 5.6 eV lower than E_F. As a result of sliding, lower energy Pb $6p_x$ states appear below E_F which accommodate the doped electrons favorably. The creation of these lower energy Pb $6p_x$ states and the existence of extra electrons on the surface are the driving force behind the sliding reconstruction. We use the Nudged Elastic Band (NEB) method[20–23] to calculate the possible barrier for this reconstruction: the barrier is negligible (< 0.1 eV per 1×1 surface unit cell) for a stoichiometric surface.

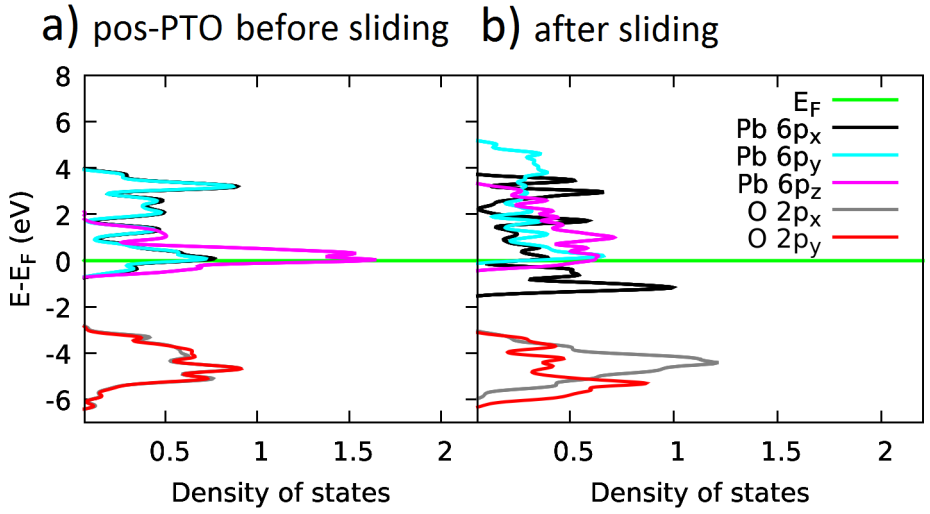

Figure 4: Projected density of states (PDOS) on the surface orbitals of of positively poled PTO. a) without sliding, b) with sliding. One should note in order to make the plot less complicated, we only show the oxygen projections which are in the valence band and only Pb projections that are in the conduction band.

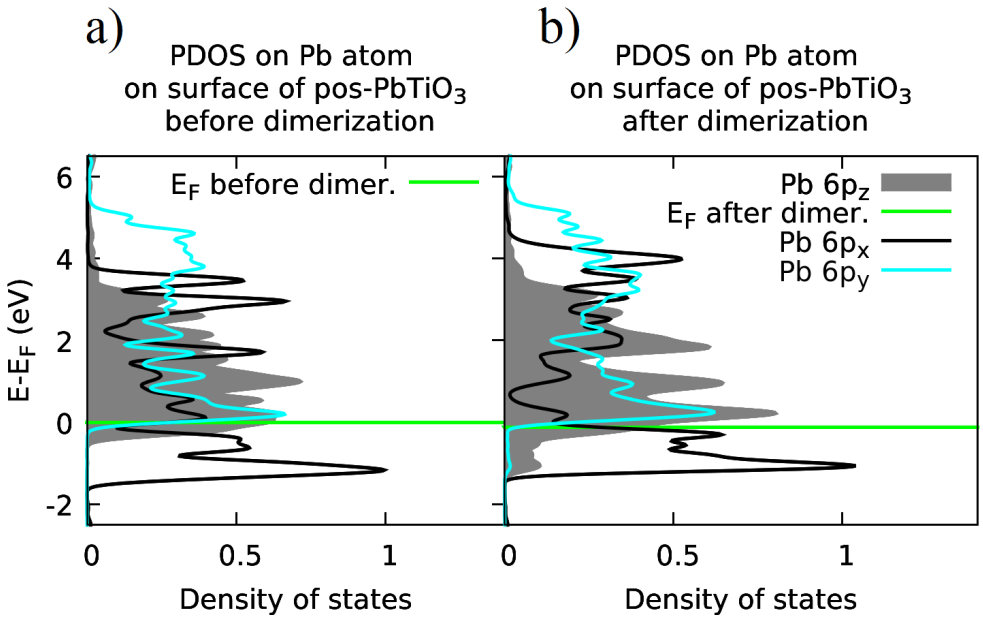

Figure 5: Projected density of states (PDOS) on a Pb atom on positively poled PTO. a) on the surface which has experienced sliding without dimerization, b) on the surface which has experienced sliding and dimerization.

Now we turn our attention to the dimerization of the surface Pb atoms. The main effect of dimerization is to increase the π bonding strength between the Pb $6p_z$ orbitals of two adjacent Pb atoms which leads to a broader Pb $6p_z$ band and consequently more lower energy Pb $6p_z$ states below E_F (see Fig 5). The standard deviations from the center of the band for Pb $6p_z$ before and after dimerization are calculated to be 1.0 eV and 1.4 eV, respectively.

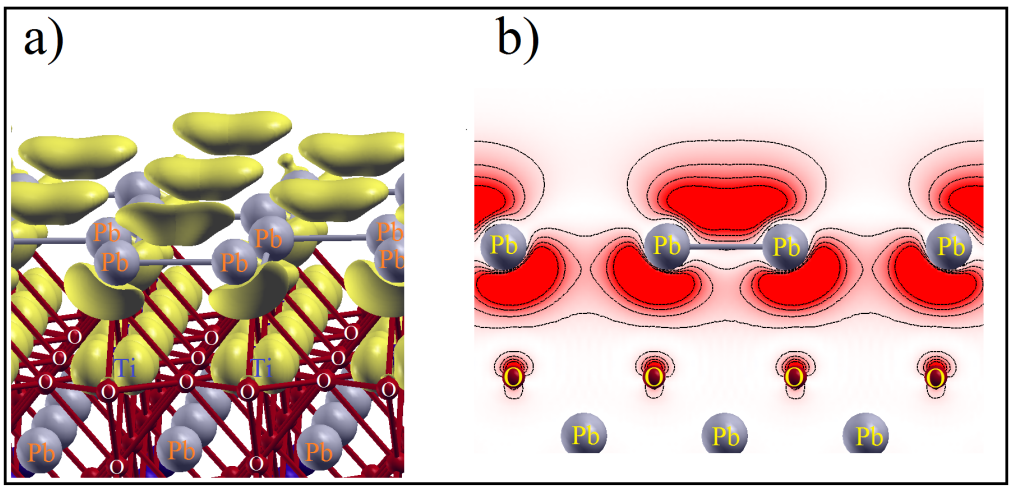

Figure 6: Integrated local density of states (ILDOS) close to the Fermi energy on the dimerized positively poled $PbTiO_3$ surface. a) 3-dimensional plot showing states close to the Fermi energy which have amplitude on both Ti 3d states below the surface and Pb 6p states on the surface. b) 2-dimensional plot in the plane that cuts through the dimerized Pb atoms.

Figure 6 shows the integrated local density of states (ILDOS) close to E_F for the surface after both dimerization and sliding of the top Pb layer have taken place. One can notice the formation of "banana bonds" between the adjacent Pb atoms which host the extra electrons on the surface. These "banana bonds" in Figures 5 and 6 are hybrids of Pb $6p_x$ and $6p_z$ orbitals.

We also relaxed the positively polarized surface using a bigger (2×2) in-plane unit cell, but this did not reduce the surface energy any further. Hence, we think a c(2×2) reconstruction is a good model for the stoichiometric positively poled PTO surface that captures the most important geometric reconstructions.

Positively-poled PTO as a CO oxidation catalyst or a TWC

As described in the main manuscript, positively-poled $PbTiO_3$ prefers to be covered with 0.5 ML O adatoms that can be provided barrierlessly by O_2 dissociation from the gas phase. These adatoms help accommodate extra doped electrons. We numerically investigate the interaction of this oxygen rich surface with 0.5 ML CO molecules, and we find that it is energetically favorable for the system by ≈ 0.35 eV per adsorbate molecule to have 0.5 ML CO_2 weakly adsorbed (0.1 eV binding energy as mentioned above) on the surface rather than having 0.5 ML CO physisorbed on the surface with 0.5 ML O adatoms. Thus the positively poled oxygen rich PTO surface can be used to oxidize CO into CO_2. The formation energy barrier has been calculated using the constrained relaxation method to be ≈ 0.2 eV. Thus positively poled PTO, once exposed to a mixed intake of O_2 and CO, might act as an effective CO oxidation catalyst. This assumes that the surface is kinetically trapped to be Pb rich and does not gradually develop 0.5 ML Pb vacancies which is predicted to be its most thermodynamically stable state[1].

Removing the surface extra oxygens using CO oxidation can create the low coverage environment necessary for NO dissociation and thus catalyzing the $NO_x \rightarrow N_2 + O_2$ reaction. Although this does not fall into the category of direct NO_x decomposition, it can potentially provide an alternative to the use of precious metals (such as Pt or Rh) which are currently being utilized in three way catalysts (TWC) in which a mixed intake of CO and NO is converted to CO_2, N_2 and O_2.

DFT Bandgap Problem and Its Effect on Our Results

The problem of the underestimation of band gaps by DFT is a well-known problem[24,25]. Consequently, the computed results presented in this work suffer from this problem as well: the experimentally measured band gap of PTO is ≈ 3.4 eV[26], but our calculations based on the GGA PW91 and GGA PBE XC functionals predict a band gap of ≈ 1.7 eV for this material. Nevertheless, we believe that the main results and cyclic schemes presented in this paper are not affected by this band gap underestimation. Our proposed cycles are mainly based on switching the surface properties from oxidizing (in positive polarization) to reducing (in negative polarization), and the basic difference in chemistry stems from the existence of electrons near the edge of the surface conduction band for positively polarized surfaces compared to having holes near the edge of the surface valence band for negatively polarized sample. More sophisticated calculations using hybrid or GW methods to correct DFT band structures of bulk ferroelectric oxides[27] show that the edge of the conduction band edge moves to higher energies compared to DFT values while the edge of the valence band edge moves to lower energies compared to DFT results. This should lead to more active electrons on the positively polarized surface and more active holes on negatively polarized surface, both of which can only enhance the difference in chemistry between reducing and oxidizing behavior.

A direct verification of this conjecture requires hybrid or GW calculations on our large slab systems which is a computationally daunting task. A simple check is to use the DFT+U method[28,29] to increase the bandgap in bulk PTO and to see its effect on the surface. We have used U=5 eV for Ti 3d and Pb 6p orbitals to compute the behavior of the ferroelectric surfaces. This value of U increases the bulk PTO band gap to 2.6 eV, and we verify that the electrons and holes on the surface behave as expected. Hence, we believe our conjecture is most likely true and our basic predictions are not upset by the DFT band gap error. However, we note that computations which have larger band gaps for the ferroelectric require thicker ferroelectric slabs in order to converge surface binding energies to the same level as before. This is because for an ultra-thin film ferroelectric of fixed thickness, increasing the band gap reduces charge transfer from the electrode to surface, so that to simulate the thick film limit corresponding to experiments one needs a thicker

ferroelectric to ensure full compensation of the surface polarization charge by charge transfer from the electrode. Thus, attempting to perform more accurate calculations with electronic structure methods that give better and enlarged band gaps (e.g., DFT+U, hybrids, GW) will require even greater computational efforts.

References

(1) Kakekhani, A.; Ismail-Beigi, S. *Journal of Materials Chemistry A* **2016**, *4*, 5235–5246.

(2) Kakekhani, A.; Ismail-Beigi, S. *ACS Catalysis* **2015**, *5*, 4537–4545.

(3) Perdew, J. P.; Burke, K.; Wang, Y. *Physical Review B* **1996**, *54*, 16533–16539.

(4) Perdew, J. P.; Burke, K.; Ernzerhof, M. *Physical Review Letters* **1996**, *77*, 3865–3868.

(5) Perdew, J. P.; Zunger, A. *Physical Review B* **1981**, *23*, 5048–5079.

(6) Tinte, S.; Stachiotti, M. G.; Rodriguez, C. O.; Novikov, D. L.; Christensen, N. E. *Physical Review B* **1998**, *58*, 11959–11963.

(7) Ziesche, P.; Kurth, S.; Perdew, J. P. *Computational Materials Science* **1998**, *11*, 122–127.

(8) Garrity, K.; Kakekhani, A.; Kolpak, A.; Ismail-Beigi, S. *Physical Review B* **2013**, *88*, 045401.

(9) Levchenko, S. V.; Rappe, A. M. *Physical Review Letters* **2008**, *100*, 256101.

(10) Chen, P.; Xu, Y.; Wang, N.; Oganov, A. R.; Duan, W. *Physical Review B* **2015**, *92*, 085432.

(11) Holscher, R.; Schmidt, W. G.; Sanna, S. *The Journal of Physical Chemistry C* **2014**, *118*, 10213–10220.

(12) Xie, Y.; Yu, H.-t.; Zhang, G.-x.; Fu, H.-g.; Sun, J.-z. *The Journal of Physical Chemistry C* **2007**, *111*, 6343–6349.

(13) Zhang, G.-X.; Xie, Y.; Yu, H.-T.; Fu, H.-G. *Journal of Computational Chemistry* **2009**, *30*, 1785–1798.

(14) Du, M.-H.; Zhang, S. B.; Northrup, J. E.; Erwin, S. C. *Physical Review B* **2008**, *78*, 155424.

(15) Kakekhani, A.; Ismail-Beigi, S.; Altman, E. I. *Surface Science* **2015**, *650*, 302–316.

(16) Peierls, S. R. E. *Quantum Theory of Solids*; Clarendon Press, 1955.

(17) Burdett, J. K.; Lee, S. *Journal of the American Chemical Society* **1983**, *105*, 1079–1083.

(18) Gou, H.; Tsirlin, A. A.; Bykova, E.; Abakumov, A. M.; Van Tendeloo, G.; Richter, A.; Ovsyannikov, S. V.; Kurnosov, A. V.; Trots, D. M.; Konopkova, Z.; Liermann, H.-P.; Dubrovinsky, L.; Dubrovinskaia, N. *Physical Review B* **2014**, *89*, 064108.

(19) Knappschneider, A.; Litterscheid, C.; George, N. C.; Brgoch, J.; Wagner, N.; Beck, J.; Kurzman, J. A.; Seshadri, R.; Albert, B. *Angewandte Chemie International Edition* **2014**, *53*, 1684–1688.

(20) Henkelman, G.; Uberuaga, B. P.; Jonsson, H. *The Journal of Chemical Physics* **2000**, *113*, 9901–9904.

(21) Mills, G.; Jonsson, H.; Schenter, G. K. *Surface Science* **1995**, *324*, 305–337.

(22) Jonsson, H.; Mills, G.; Jacobsen, K. W. *Nudged Elastic Band Method for Finding Minimum Energy Paths of Transitions*; 385.

(23) Mills, G.; Jónsson, H. *Physical Review Letters* **1994**, *72*, 1124–1127.

(24) Grüning, M.; Marini, A.; Rubio, A. *The Journal of Chemical Physics* **2006**, *124*, 154108.

(25) Rinke, P.; Janotti, A.; Scheffler, M.; Van de Walle, C. G. *Physical Review Letters* **2009**, *102*, 026402.

(26) Piskunov, S.; Heifets, E.; Eglitis, R. I.; Borstel, G. *Computational Materials Science* **2004**, *29*, 165–178.

(27) Bilc, D. I.; Orlando, R.; Shaltaf, R.; Rignanese, G.-M.; Íñiguez, J.; Ghosez, P. *Physical Review B* **2008**, *77*, 165107.

(28) Cococcioni, M.; de Gironcoli, S. *Physical Review B* **2005**, *71*, 035105.

(29) Hu, Z.; Metiu, H. *The Journal of Physical Chemistry C* **2011**, *115*, 5841–5845.